Acta Crystallographica Section F
Structural Biology and Crystallization Communications
ISSN 1744-3091

Structure of the RBD-PRDI fragment of the antiterminator protein GlcT

Sebastian Himmel,[a]‡ Christian Grosse,[b]‡ Sebastian Wolff,[a] Claudia Schwiegk[a] and Stefan Becker[a]*

[a]Department of NMR-based Structural Biology, Max Planck Institute for Biophysical Chemistry, Göttingen, Germany, and [b]Lehrstuhl für Strukturchemie, Universität Göttingen, Göttingen, Germany

‡ These authors contributed equally.

Correspondence e-mail: sabe@nmr.mpibpc.mpg.de

Received 27 March 2012
Accepted 7 May 2012

PDB Reference: RBD-PRDI fragment of GlcT, 3rio.

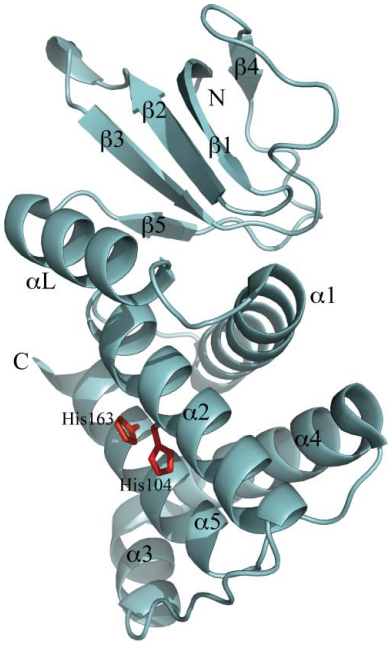

© 2012 International Union of Crystallography
All rights reserved

GlcT is a transcriptional antiterminator protein that is involved in regulation of glucose metabolism in *Bacillus subtilis*. Antiterminator proteins bind specific RNA sequences, thus preventing the formation of overlapping terminator stem-loops. The structure of a fragment (residues 3–170) comprising the RNA-binding domain (RBD) and the first regulatory domain (PRDI) of GlcT was solved at 2.0 Å resolution with one molecule in the asymmetric unit. The two domains are connected by a helical linker. Their interface is mostly constituted by hydrophobic interactions.

1. Introduction

Glucose is the preferred carbon and energy source of *Bacillus subtilis* and several other bacteria such as *Escherichia coli* (Postma *et al.*, 1993). To enter the glycolysis pathway in these bacteria, the glucose is phosphorylated during sugar uptake by a phosphoenolpyruvate:sugar phosphotransferase system (PTS). This system consists of two energy-coupling proteins, enzyme I (EI) and histidine-containing phosphocarrier protein HPr, and the carbohydrate-specific permease enzyme II (EII). These enzymes are co-transcribed from the *ptsGHI* operon (Stülke *et al.*, 1997), which is regulated by the transcriptional antiterminator protein GlcT in a glucose-dependent manner. GlcT belongs to the well characterized BglG/SacY family of antiterminator proteins (Mahadevan & Wright, 1987; Crutz & Steinmetz, 1992). These proteins generally consist of an N-terminal effector domain termed the RNA-binding domain (RBD) and two contiguous C-terminal regulatory domains: PTS regulatory domains I (PRDI) and II (PRDII). The RBD interacts specifically with a ribonucleic antiterminator sequence (RAT). The PRD domains control the function of the RBD depending on their phosphorylation state (van Tilbeurgh & Declerck, 2001). GlcT is intrinsically in an active dimeric state. HPr-dependent phosphorylation of specific histidine residues in PRDII further stabilizes the dimer, thus enhancing the activity of GlcT. The dimeric GlcT binds the RAT that overlaps with a transcription terminator sequence, thus preventing the formation of the terminator stem-loop and allowing transcriptional elongation to proceed (Langbein *et al.*, 1999). In the absence of glucose, EII phosphorylates specific histidine residues in PRDI, resulting in weak dimer formation that is possibly in equilibrium with a monomeric inactive state of GlcT that is incompetent for interaction with the RAT, resulting in transcriptional termination (van Tilbeurgh & Declerck, 2001; Schmalisch *et al.*, 2003; Graille *et al.*, 2005).

NMR and crystal structures of the RBDs of the homologous antiterminators SacY and LicT (Manival *et al.*, 1997; van Tilbeurgh *et al.*, 1997; Yang *et al.*, 2002) have been solved. These structures show that the RBD forms a homodimer. The crystal structure of the native PRDI-PRDII fragment of LicT (Graille *et al.*, 2005) is supposed to represent the inactive state of LicT, as its dimerization is only mediated by a relatively small interface between the PRDI domains opposite to the PRDI-PRDII fragment that carries the His207Asp/His269Asp histidine phosphorylation-mimicking double mutant in

Table 1
X-ray data collection and phasing.

Values in parentheses are for the outer resolution shell.

	Native	Peak	Inflection	High-energy remote
Data-collection statistics				
Beamline	X10SA, Swiss Light Source			
Wavelength (Å)	0.9999	0.9792	0.9794	0.9715
Detector	Pilatus 6M			
Crystal-to-detector distance (mm)	300	390		
Rotation range per image (°)	0.5	0.2	0.2	0.2
Total rotation range (°)	180	120	100	100
Exposure time per image (s)	0.25	0.1	0.1	0.1
Attenuation (%)	85	90	90	90
Resolution (Å)	2.0 (2.04–2.00)	2.40 (2.44–2.40)	2.70 (2.75–2.70)	2.70 (2.75–2.70)
Space group	$P2_12_12_1$			
Unit-cell parameters (Å)	a = 35.88, b = 47.66, c = 126.57	a = 35.55, b = 46.91, c = 126.28	a = 35.61, b = 47.07, c = 126.63	a = 35.59, b = 47.42, c = 126.52
Mosaicity (°)	0.083	0.262	0.337	0.325
Total reflections	47725	37248	21856	21902
Unique reflections	15233	8808	5985	5979
Completeness (%)	98.7 (92.7)	99.7 (97.9)	95.0 (94.1)	95.1 (93.9)
Multiplicity	3.09 (3.15)	4.22 (4.35)	3.47 (3.36)	3.48 (3.39)
Mean $I/\sigma(I)$	9.15 (2.25)	10.85 (2.69)	10.55 (2.88)	11.81 (3.24)
$R_{\rm r.i.m.}$† (%)	8.74 (35.55)	7.37 (29.73)	7.58 (27.77)	6.77 (24.69)
Substructure solution (*SHELX*)				
d'/sig	—	1.37 at 6.0–5.0 Å	1.2 at 6.0–5.0 Å	1.24 at 8.0–6.0 Å
$CC_{\rm anom}$ (∞–8.0 Å)	—	81.4	82.7	60.3
No. of sites	4			
CC (all/weak)	47.69/38.88			
PATFOM	42.45			

† $R_{\rm r.i.m.} = \sum_{hkl}\{N(hkl)/[N(hkl)-1]\}^{1/2}\sum_i |I_i(hkl) - \langle I(hkl)\rangle|/\sum_{hkl}\sum_i I_i(hkl)$, where N is the redundancy, $I_i(hkl)$ is the ith observation of reflection hkl and $\langle I(hkl)\rangle$ is the weighted average intensity for all observations i of reflection hkl.

PRDII and shows a dimerization mode with extended interfaces between both the PRDI and the PRDII domains (van Tilbeurgh *et al.*, 2001). Here, we have solved the crystal structure of the GlcT RBD-PRDI fragment in a monomeric state. We analyzed this structure with regard to the structural data available for LicT and SacY and found that the conformation of this structure is not compatible with the RBD and PRDI-PRDII homodimer structures deposited in the PDB. However, our new structure contains features that are consistent with the inactive state of the LicT RBD-PRDI fragment.

2. Materials and methods

2.1. Cloning, expression and purification

Residues 2–170 of GlcT encoding the RBD and PRDI domains with an additional N-terminal expression tag comprising the sequence MTKELRIV were amplified by PCR from the *B. subtilis* genome (strain 168; Barbe *et al.*, 2009) using the primers 5′-CGAGGATCCCATATGACAAAGGAGCTGAGGATCGTG-3′ and 5′-GGAAAGCTTGAATTCTCAGTTTGTCAACGCTGAATGGATATGC-3′. The amplified insert was digested with *Bam*HI/*Eco*RI and cloned into a modified pET28a expression vector (Novagen) containing a His_7 tag and a TEV cleavage site upstream of the multiple cloning site of the vector. The RBD-PRDI expression construct was transformed into *E. coli* strain BL21 (DE3). Protein expression was carried out at 295 K by induction with 0.5 m*M* isopropyl β-D-1-thiogalactopyranoside. The cells were harvested 18 h after induction. Selenomethionine-labelled RBD-PRDI was overexpressed in minimal medium supplemented with selenomethionine according to the EMBL protein-expression group (http://embl-heidelberg.de).

The cells were resuspended in lysis buffer (200 m*M* NaCl, 50 m*M* Tris–HCl pH 7.9, 5 m*M* imidazole). Lysis was achieved by ultrasonication followed by centrifugation at 27 000*g* and 277 K. Nucleic acids were removed by polyethyleneimine precipitation [0.2%(*v*/*v*) final concentration]. The recombinant RBD-PRDI was purified from the supernatant by immobilized metal-affinity chromatography on Ni^{2+}–NTA agarose resin (Qiagen). The fusion protein was subsequently cleaved by proteolytic digestion with recombinant tobacco etch virus (TEV) protease. The RBD-PRDI fragment was separated from the fusion tag by size-exclusion chromatography on a Superdex 75 (16/60) gel-filtration column (GE Healthcare) equilibrated with 200 m*M* NaCl, 50 m*M* Tris–HCl pH 7.4, 2 m*M* DTT. Prior to crystallization, the purified protein was dialyzed against 10 m*M* Tris–HCl pH 8.0, 200 m*M* NaCl, 10%(*v*/*v*) glycerol, 2 m*M* DTT and concentrated to 7.9 mg ml^{-1}.

2.2. Crystallization, data collection and structure determination

Crystals of native and selenomethionine-labelled RBD-PRDI were obtained at 293 K by sitting-drop vapour diffusion. The crystals grew during one week from 200 nl drops composed of equal volumes of protein solution and mother liquor consisting of 6%(*w*/*v*) PEG 3350, 0.11 *M* sodium formate pH 6.0. Prior to data collection, crystals were cryoprotected by transferring them into their reservoir solution supplemented with 30%(*v*/*v*) glycerol followed by flash-cooling them in liquid nitrogen. A native data set and three MAD data sets (peak, inflection and high-energy remote) were collected from crystals of selenomethionine-derivatized GlcT RBD-PRDI at SLS Villigen, Switzerland (beamline PXII, Pilatus 6M detector; Broennimann *et al.*, 2006). All data were processed using *XDS* (Kabsch, 2010) and scaled with *SADABS* (Bruker AXS, Madison, Wisconsin, USA). Space-group determination, data merging and statistical analysis was carried out by *XPREP* (Bruker AXS, Madison, Wisconson, USA). Statistics of data-collection and phasing are summarized in Table 1.

Both native and selenomethionine-labelled protein crystallized in space group $P2_12_12_1$, with one molecule per asymmetric unit. The structure was solved by multiwavelength anomalous dispersion (MAD) and normalized difference structure factors were calculated

using *SHELXC*. Substructure solution using *SHELXD* (Schneider & Sheldrick, 2002) identified four selenium sites, consistent with the presence of one monomer in the asymmetric unit. With the MAD phases calculated from these sites, the native data set was used for phase extension, density modification and main-chain autotracing with a beta test version of *SHELXE* (Sheldrick, 2008). *SHELXE* traced 83% of the residues in five chains. 50 cycles of automatic model building alternating with structure refinement with *ARP*/*wARP* (Perrakis *et al.*, 1999) resulted in the modelling of 91% of the residues. Refinement was initially performed by positional and *B*-factor refinement in *REFMAC*5 (Murshudov *et al.*, 2011) and finally with *BUSTER* (Bricogne *et al.*, 2011) alternating with manual model building in *Coot* (Emsley *et al.*, 2010). Refinement statistics are given in Table 2.

2.3. Structural alignments

Superpositions of structural models were performed by secondary-structure matching (*SSM*; Krissinel & Henrick, 2004) of protein backbone C^{α} atoms as implemented in *Coot* (Emsley *et al.*, 2010).

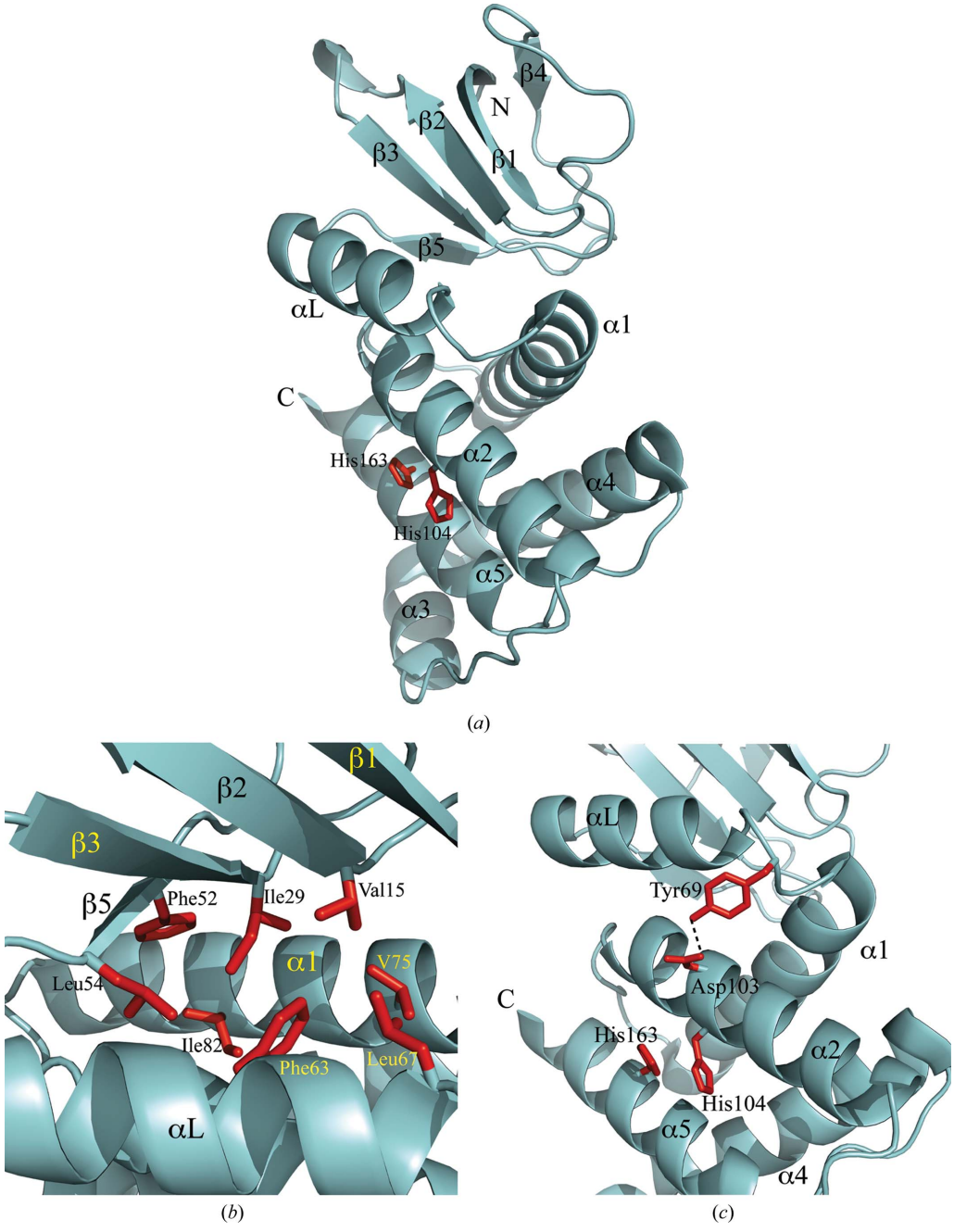

Figure 1
Crystal structure of GlcT RBD-PRDI. (*a*) Overall structure of the GlcT RBD-PRDI$_{3–170}$ fragment. The helical linker between the RBD (top) and the PRDI domain (bottom) is named αL. The histidine residues 104 and 163 that are possibly phosphorylated upon inactivation are displayed as red stick models. (*b*) Close-up view of the intramolecular interface between the RBD and the PRDI domain. Residues constituting hydrophobic interactions between the domains are coloured in red. (*c*) Close-up view of the region comprising residues Asp103 and Tyr69 that form a strong hydrogen bond.

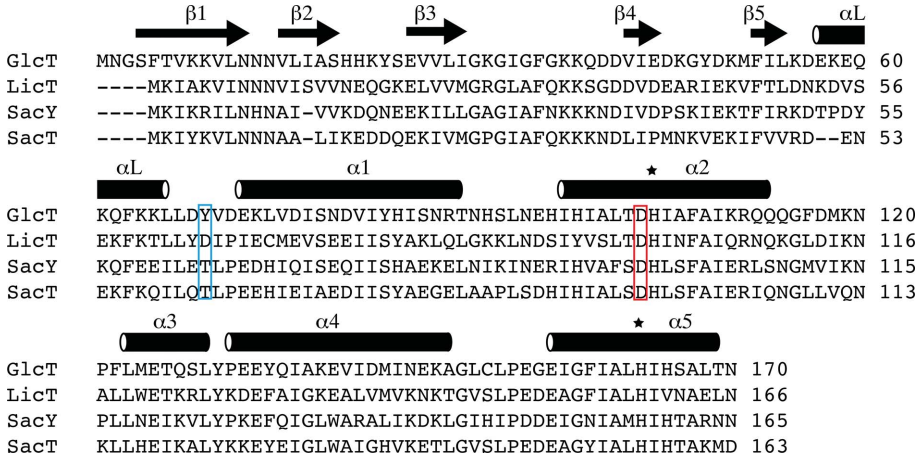

Figure 2
Sequence alignment of the RBD-PRDI domain regions of the antiterminator proteins GlcT (UniProt O31691), LicT (UniProt P39805), SacY (UniProt P15401) and SacT (UniProt P26212) from *B. subtilis*. The alignment was performed with *Clustal Omega* (Sievers *et al.*, 2011; Goujon *et al.*, 2010). The sequence identities obtained by *LALIGN* (Huang & Miller, 1991) between the fragments of GlcT and LicT, of GlcT and SacY and of GlcT and SacT are 39.6, 39.6 and 40.4%, respectively. The secondary structure obtained from the RBD-PRDI crystal structure in this study is shown above the alignment. The conserved Asp103 in GlcT is indicated by a red box. Tyr69 from GlcT, which is not conserved, is depicted by a blue box. The conserved histidine residues that are postulated to be specifically phosphorylated upon inactivation are indicated by stars.

3. Results and discussion

3.1. The overall structure

The structure was solved at a resolution of 2 Å with one monomer in the asymmetric unit. The final model of GlcT RBD-PRDI consists of one protein chain comprising residues 3–170 (Fig. 1*a*). The model also contained six glycerol and 135 water molecules. The crystallized protein fragment consists of the N-terminal RBD (residues 3–61) and the contiguous PRDI domain (residues 71–170). The two domains are connected by a mostly helical (residues 56–67) linker (residues 55–70). The RBD is composed of a four-stranded antiparallel β-sheet, while the PRDI domain forms a compact five-helix bundle. Individually, both domains are structurally very similar to the structures of homologous proteins. The root-mean-square deviation (r.m.s.d.) between the GlcT RBD and the best representative conformer of the NMR structure of the LicT RBD (PDB entry 1l1c; Yang *et al.*, 2002) is 1.23 Å (alignment of 38 backbone C^{α} atoms from each RBD; residues 5–42 of the LicT RBD and residues 9–56 of the GlcT RBD). Thus, the basic fold is well preserved between the two RBDs. The r.m.s.d.s between the GlcT PRDI domain and the LicT PRDI domain (PDB entries 1h99 and 1tlv; van Tilbeurgh *et al.*, 2001; Graille *et al.*, 2005) were 1.14 Å for 1h99 and 1.13 Å for 1tlv. In the superpositions, 94 backbone C^{α} atoms were used from each PRDI (residues 73–166 of the GlcT PRDI and residues 69–162 of the LicT PRDI). Despite this high structural similarity, we were not able to solve the structure of the RBD-PRDI fragment of GlcT by molecular replacement. A reason for this failure may be that only NMR structures for the RBDs of LicT and SacY are available in the PDB (PDB entries 1auu and 1l1c; Manival *et al.*, 1997; Yang *et al.*, 2002), although progress has recently been reported in using NMR models for molecular replacement (Mao *et al.*, 2011).

Owing to the space group ($P2_12_12_1$), no symmetry-related homodimer was identified in our GlcT RBD-PRDI structure. In contrast, the retention volume of the RBD-PRDI fragment determined by size-exclusion chromatography was consistent with a dimeric state in solution (data not shown). Also, the molecular weight of the protein determined by electrospray ionization mass spectrometry (ESI-MS) was consistent with the nonphosphorylated state that should form a dimer (see Supplementary Fig. S1[1]). In addition, the GlcT RBD-PRDI fragment interacted with an RNA fragment comprising the specific RAT recognition sequence in a bandshift assay (see Supplementary Fig. S2[1]). The homologous RBD-PRDI fragment of LicT exhibited two peaks in analytical size-exclusion chromatography consistent with a monomer and a dimer (Déméné *et al.*, 2008). Thus, the crystallization condition of the GlcT fragment obviously favoured the monomer despite its dimeric state in solution. It is possible that the crystallization at pH 6.0 may have resulted in the protonation of some residues in the dimerization interface, resulting in destabilization of the dimer. Specifically, the side chains of His104 in α-helix 2 and His163 in α-helix 5 (Fig. 1) may be protonated at this pH, which is approximately equivalent to the theoretical pI of the side chain of free histidine. Both histidines are possibly phosphorylated upon inactivation of GlcT (Bachem & Stülke, 1998; Schmalisch *et al.*, 2003). In the PRDI of the active dimer of LicT (van Tilbeurgh *et al.*, 2001), the homologous histidine residues 100 and 159 (Fig. 2) form part of the dimer interface. Assuming that destabilization of the dimer

Table 2
Refinement and model statistics.

Resolution (Å)	2.0
Final *R* factor† (%)	
Working set	21.0
Working set + test set	21.12
R_{free}‡ (%)	24.65
R.m.s.d. bond lengths (Å)	0.01
R.m.s.d. bond angles (°)	1.22
Mean *B* value (Å^2)	
Main-chain atoms	25.5
Side-chain atoms	28.7
Solvent content (%)	51.87
No. of protein residues	168
No. of glycerol molecules	6
No. of water molecules	135
Ramachandran plot (% of residues in)	
Most favoured regions	98.2
Additionally allowed regions	1.8
Disallowed regions	0

† $R = \sum_{hkl} ||F_{obs}| - |F_{calc}|| / \sum_{hkl} |F_{obs}|$, where F_{obs} and F_{calc} are the observed and calculated structure factors, respectively. ‡ R_{free} was determined using 5% of the data (Brünger, 1992).

[1] Supplementary material has been deposited in the IUCr electronic archive (Reference: WD5182).

interface by phosphorylation of these residues is based on charge repulsion, protonation of these residues might have a similar destabilizing effect.

3.2. Interaction between the RBD and the PRDI domain

The intramolecular interface between the RBD and the PRDI domain, including the linker helix, covers 790 Å^2. Apart from polar interactions at the surface, the interface is mostly constituted by hydrophobic interactions between residues from both domains (Fig. 1*b*). Such a tight interaction between RBD and PRDI was also indicated for LicT by superposition of the ^{15}N–^{1}H HSQC spectra of the isolated RBD, which forms a dimer in solution and in crystal structures (Manival *et al.*, 1997; van Tilbeurgh *et al.*, 1997; Yang *et al.*, 2002), and the RBD-PRDI fragment of LicT (Déméné *et al.*, 2008). These authors demonstrated that many RBD resonance peaks were

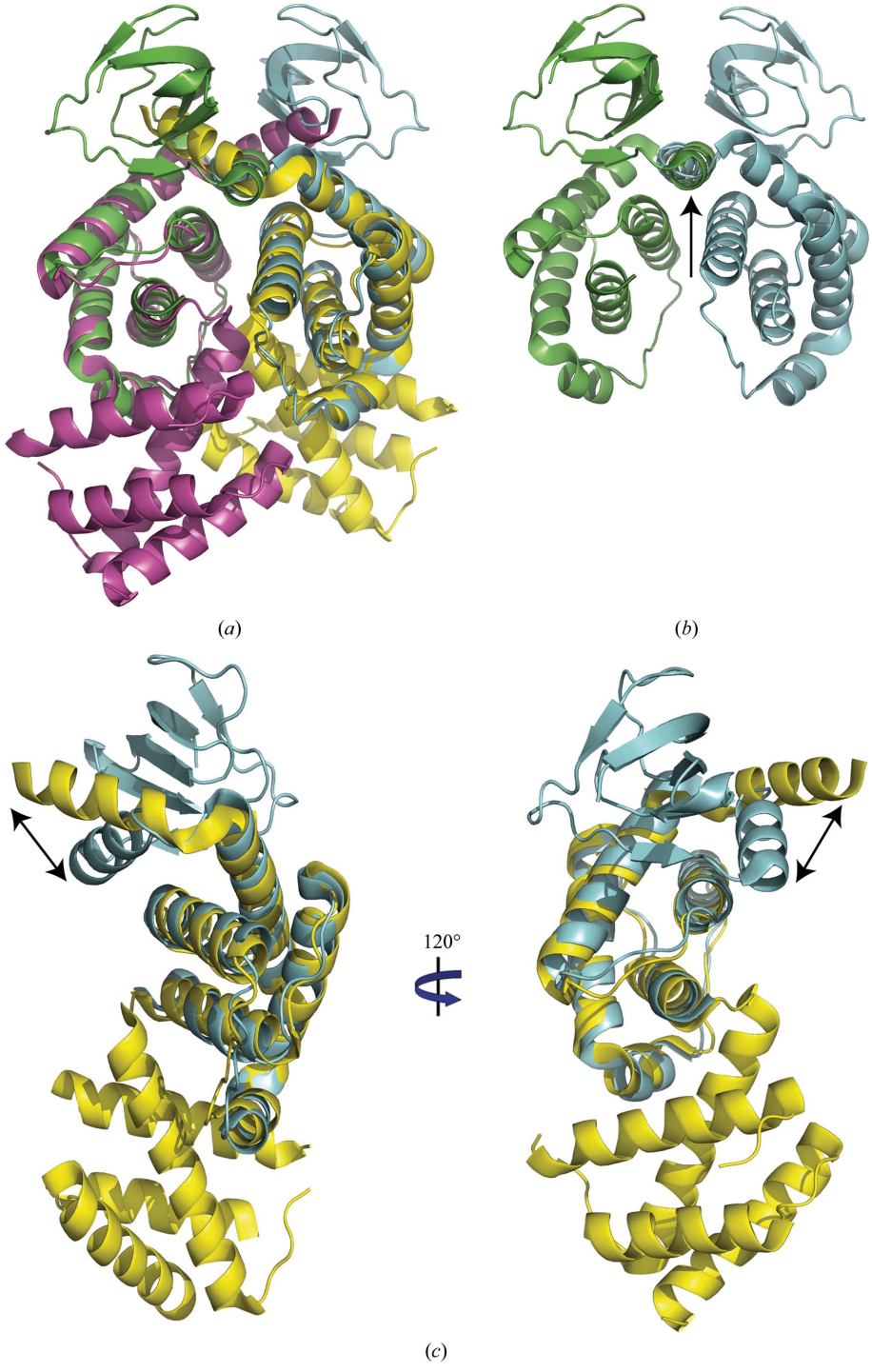

Figure 3
Superposition of GlcT RBD-PRDI with LicT. (*a*) Superposition of the GlcT RBD-PRDI model (cyan and green) with the inactive PRDI-PRDII dimer of LicT (yellow and purple). (*b*) GlcT RBD-PRDI dimer resulting from (*a*). The clashing linker helices are indicated by an arrow. (*c*) Side views of (*a*) showing the superposition of a GlcT RBD-PRDI monomer (cyan) with a PRDI-PRDII monomer from LicT (yellow). The double-headed arrow indicates the different orientations of the linker helix in the models.

shifted in the presence of the PRDI. Next, they also found that the RBD-PRDI linker of LicT was helical based on numerous H_N–H_N NOEs in this region. Overall, the NMR data for LicT RBD-PRDI fitted very well to the structural features of our GlcT RBD-PRDI crystal structure, namely an extended intramolecular interface between the RBD and the PRDI and a helical linker connecting RBD and PRDI. For LicT these structural features were assigned to its inactive state (Déméné *et al.*, 2008). From the coincidence of these data with our crystal structure, we conclude that the conformation of our GlcT RBD-PRDI fragment is consistent with the inactive state of this regulatory protein.

In the constitutively activated dimeric LicT RBD-PRDI D99N mutant the linker helix between RBD and PRDI has changed to coil (Déméné *et al.*, 2008), suggesting that activation of LicT is accompanied by a helix-to-coil transition in the linker. Interestingly, the Asp99 residue of LicT is highly conserved in GlcT and also in the homologous antiterminator proteins SacY and SacT (Fig. 2). In our GlcT RBD-PRDI structure the side-chain carboxyl group of the homologous residue Asp103 in helix 2 of PRDI forms a hydrogen bond to the side-chain hydroxyl group of Tyr69 located in the loop region between the linker helix and helix 1 of PRDI (Fig. 1c). The Asp103 carboxyl group is probably deprotonated owing to its location at the protein surface, resulting in a strong hydrogen bond to Tyr69 that is located in the extended linker region connecting the linker helix to helix 1 of PRDI (Fig. 1*c*). Tyr69 of GlcT is not strictly conserved in other antiterminator proteins (Fig. 2). Nevertheless, a strong hydrogen bond as observed between the conserved Asp103 and Tyr69 in GlcT is highly probably an intricate feature of the inactive state of all antiterminator proteins, while activation is accompanied by the breaking of this hydrogen bond, as demonstrated for the homologous D99N mutant in LicT (Déméné *et al.*, 2008).

3.3. Superposition with the inactive LicT PRDI-PRDII dimer

As our GlcT RBD-PRDI structure most probably represents an inactive state of GlcT, it seemed reasonable to superpose our GlcT RBD-PRDI monomer with the inactive LicT PRDI-PRDII dimer. Superposition of this dimer (PDB entry 1tlv; Graille *et al.*, 2005) with two GlcT RBD-PRDI monomers *via* the structurally highly similar PRDI domains (see above) resulted in severe clashes between the linker helices of the opposite RBD-PRDI monomers (Figs. 3*a* and 3*b*). Manual rotation of the linker helix in our GlcT RBD-PRDI model to obtain the same orientation as the linker helix in the inactive LicT PRDI-PRDII structure (Fig. 3*c*) resulted in an even more severe clash between the RBD monomers. Thus, our monomeric GlcT RBD-PRDI structure is not compatible with the dimeric inactive state of the LicT PRDI-PRDII fragment. Severe clashes were also obtained for superpositions of GlcT RBD-PRDI monomers with the active LicT PRDI-PRDII and with the available dimeric RBD structures (not shown).

While the GlcT RBD-PRDI structure does not fit to the antiterminator structures deposited in the PDB to date, this new structure might represent the hypothesized monomeric inactive form of antiterminator proteins (van Tilbeurgh & Declerck, 2001; Déméné *et al.*, 2008). At the same time, the size of the interface between the RBD and the PRDI mentioned above implies biological relevance (Ponstingl *et al.*, 2000). Overall, our GlcT RBD-PRDI structure allows the first detailed view of the mutual orientation of the RBD and PRDI, most probably in the inactive monomeric state of GlcT.

This work was supported by the Max Planck Society. We are grateful to George Sheldrick, Jörg Stülke and Christian Griesinger for generous support. We thank Tobias Beck and Tim Grüne for help with data collection and advice on data processing and the staff scientists of PXII at SLS for support. We thank Gerhard Wolf and Kerstin Overkamp for ESI-MS measurements.

References

Bachem, S. & Stülke, J. (1998). *J. Bacteriol.* **180**, 5319–5326.
Barbe, V., Cruveiller, S., Kunst, F., Lenoble, P., Meurice, G., Sekowska, A., Vallenet, D., Wang, T., Moszer, I., Médigue, C. & Danchin, A. (2009). *Microbiology*, **155**, 1758–1775.
Bricogne, G., Blanc, E., Brandl, M., Flensburg, C., Keller, P., Paciorek, W., Roversi, P., Sharff, A., Smart, O. S., Vonrhein, C. & Womack, T. O. (2011). *BUSTER* v.2.8.0. Cambridge: Global Phasing Ltd.
Broennimann, C., Eikenberry, E. F., Henrich, B., Horisberger, R., Huelsen, G., Pohl, E., Schmitt, B., Schulze-Briese, C., Suzuki, M., Tomizaki, T., Toyokawa, H. & Wagner, A. (2006). *J. Synchrotron Rad.* **13**, 120–130.
Brünger, A. T. (1992). *Nature (London)*, **355**, 472–475.
Crutz, A. M. & Steinmetz, M. (1992). *J. Bacteriol.* **174**, 6087–6095.
Déméné, H., Ducat, T., De Guillen, K., Birck, C., Aymerich, S., Kochoyan, M. & Declerck, N. (2008). *J. Biol. Chem.* **283**, 30838–30849.
Emsley, P., Lohkamp, B., Scott, W. G. & Cowtan, K. (2010). *Acta Cryst.* D**66**, 486–501.
Goujon, M., McWilliam, H., Li, W., Valentin, F., Squizzato, S., Paern, J. & Lopez, R. (2010). *Nucleic Acids Res.* **38**, W695–W699.
Graille, M., Zhou, C.-Z., Receveur-Bréchot, V., Collinet, B., Declerck, N. & van Tilbeurgh, H. (2005). *J. Biol. Chem.* **280**, 14780–14789.
Huang, X. & Miller, W. (1991). *Adv. Appl. Math.* **12**, 337–357.
Kabsch, W. (2010). *Acta Cryst.* D**66**, 125–132.
Krissinel, E. & Henrick, K. (2004). *Acta Cryst.* D**60**, 2256–2268.
Langbein, I., Bachem, S. & Stülke, J. (1999). *J. Mol. Biol.* **293**, 795–805.
Mahadevan, S. & Wright, A. (1987). *Cell*, **50**, 485–494.
Manival, X., Yang, Y., Strub, M. P., Kochoyan, M., Steinmetz, M. & Aymerich, S. (1997). *EMBO J.* **16**, 5019–5029.
Mao, B., Guan, R. & Montelione, G. T. (2011). *Structure*, **19**, 757–766.
Murshudov, G. N., Skubák, P., Lebedev, A. A., Pannu, N. S., Steiner, R. A., Nicholls, R. A., Winn, M. D., Long, F. & Vagin, A. A. (2011). *Acta Cryst.* D**67**, 355–367.
Perrakis, A., Morris, R. & Lamzin, V. S. (1999). *Nature Struct. Biol.* **6**, 458–463.
Ponstingl, H., Henrick, K. & Thornton, J. M. (2000). *Proteins*, **41**, 47–57.
Postma, P. W., Lengeler, J. W. & Jacobson, G. R. (1993). *Microbiol. Rev.* **57**, 543–594.
Schmalisch, M. H., Bachem, S. & Stülke, J. (2003). *J. Biol. Chem.* **278**, 51108–51115.
Schneider, T. R. & Sheldrick, G. M. (2002). *Acta Cryst.* D**58**, 1772–1779.
Sheldrick, G. M. (2008). *Acta Cryst.* A**64**, 112–122.
Sievers, F., Wilm, A., Dineen, D., Gibson, T. J., Karplus, K., Li, W., Lopez, R., McWilliam, H., Remmert, M., Söding, J., Thompson, J. D. & Higgins, D. G. (2011). *Mol. Syst. Biol.* **7**, 539.
Stülke, J., Martin-Verstraete, I., Zagorec, M., Rose, M., Klier, A. & Rapoport, G. (1997). *Mol. Microbiol.* **25**, 65–78.
Tilbeurgh, H. van & Declerck, N. (2001). *Curr. Opin. Struct. Biol.* **11**, 685–693.
Tilbeurgh, H. van, Le Coq, D. & Declerck, N. (2001). *EMBO J.* **20**, 3789–3799.
Tilbeurgh, H. van, Manival, X., Aymerich, S., Lhoste, J. M., Dumas, C. & Kochoyan, M. (1997). *EMBO J.* **16**, 5030–5036.
Yang, Y., Declerck, N., Manival, X., Aymerich, S. & Kochoyan, M. (2002). *EMBO J.* **21**, 1987–1997.